Identification of the myogenetic oligodeoxynucleotides (myoDNs) that promote differentiation of skeletal muscle myoblasts by targeting nucleolin

Sayaka Shinji[1], Koji Umezawa[2,3], Yuma Nihashi[4], Shunichi Nakamura[1], Takeshi Shimosato[1,2,3,4], Tomohide Takaya[1,2,3,4]*

[1]Department of Agriculture, Graduate School of Science and Technology, Shinshu University, Nagano, Japan;

[2]Department of Agricultural and Life Science, Faculty of Agriculture, Shinshu University, Nagano, Japan;

[3]Department of Biomolecular Innovation, Institute for Biomedical Sciences, Shinshu University, Nagano, Japan;

[4]Department of Science and Technology, Graduate School of Medicine, Science and Technology, Shinshu University, Nagano, Japan

*For correspondence:

Tomohide Takaya

ttakaya@shinshu-u.ac.jp.

Running title: Myogenetic oligodeoxynucleotides promote myoblast differentiation

Abstract

Herein we report that the 18-base telomeric oligodeoxynucleotides (ODNs) designed from the *Lactobacillus rhamnosus* GG genome promote differentiation of skeletal muscle myoblasts which are myogenic precursor cells. We termed these myogenetic ODNs (myoDNs). The activity of one of the myoDNs, iSN04, was independent of Toll-like receptors, but dependent on its conformational state. Molecular simulation and iSN04 mutants revealed stacking of the 13-15th guanines as a core structure for iSN04. The alkaloid berberine bound to the guanine stack and enhanced iSN04 activity, probably by stabilizing and optimizing iSN04 conformation. We further identified nucleolin as an iSN04-binding protein. Results showed that iSN04 antagonizes nucleolin, increases the levels of p53 protein translationally suppressed by nucleolin, and eventually induces myotube formation by modulating the expression of genes involved in myogenic differentiation and cell cycle arrest. This study shows that bacterial-derived myoDNs serve as aptamers and are potential nucleic acid drugs directly targeting myoblasts.

Keywords

oligodeoxynucleotide, berberine, nucleolin, skeletal muscle myoblast, myogenic differentiation

Introduction

Skeletal muscle myoblasts are myogenic precursor cells that play a central role during muscle development and regeneration. In the first step of these processes, muscle stem cells called satellite cells on myofibers are activated into myoblasts. After several rounds of division, myoblasts differentiate into myocytes, which is led by myogenic transcription factors such as MyoD and myogenin. Myocytes then fuse to form multi-nuclear myotubes to generate or restore myofibers (Dumont et al., 2015). However, the differentiation ability of myoblasts declines due to aging or diseases. Aged murine myoblasts tend to differentiate into the fibrogenic lineage by the activation of the canonical Wnt pathway (Brack et al., 2007). The myoblasts isolated from the chronic kidney disease mice model showing muscle atrophy display attenuated MyoD expression and myotube formation (Zhang et al., 2010). Cancer-conditioned media inhibit myogenic differentiation by upregulating C/EBPβ in the murine myoblast cell line C2C12 (Marchildon et al., 2015). Such hypoactivities of myoblasts are considered to be one of the reasons for the development of muscle atrophy (Fukada, 2018; McCormick and Vasilaki, 2018). Therefore, myoblast differentiation can be a clinical target for sarcopenia, disease-related muscle wasting, and cancer cachexia which are risk factors for mortality (Anker et al., 1997; Rubin, 2003; Carrero et al., 2008).

Several molecules have been identified that facilitate myogenic differentiation. Histone deacetylase inhibitors (HDACIs), trichostatin A

(TSA) and valproic acid (VPA), promote myotube formation by inducing follistatin in myoblasts (Iezzi et al., 2004). However, TSA and VPA are non-specific HDACIs that affect a broad range of biological processes in vivo. Recent studies have reported that the combined treatment of ursolic acid (UA) with leucine (Kim et al., 2015), and a single treatment of an oleanolic acid (OA) derivative (Cui et al., 2019) potentiates differentiation of C2C12 cells. As the half-lives of UA in plasma and OA in serum are less than 1 h (Chen et al., 2011; Li et al., 2012), their pharmacokinetic parameters need to be improved for clinical application.

Nucleic acids have tremendous potential for use in next-generation drugs. They are chemically synthesized, stable, and modifiable molecules that can access diverse targets with high specificities. Complementary antisense oligonucleotides modulate gene expression by degrading mRNAs, trapping microRNAs, or correcting splicing events (Quemener et al., 2020). Other types of oligonucleotides serve as aptamers that specifically interact with their target proteins (Wang et al., 2019). Furthermore, many immunomodulatory oligodeoxynucleotides (ODNs) from microbial and autologous DNA sequences have been reported. ODNs with unmethylated CpG motifs (CpG-ODNs) serve as ligands for Toll-like receptor (TLR) 9 and initiate an inflammatory cascade (Vollmer and Krieg, 2009). In contrast, inhibitory ODNs (iODNs) representatively expressing telomeric elements suppress immunological reactions depending on TLR3, TLR7, and TLR9 (Klinman et al., 2008; Sackesen et al., 2013). At present, CpG-ODNs and iODNs are anticipated to

92 be effective drugs for sepsis and allergic diseases (Yamamoto et al., 2017;
93 Wang et al., 2015).

94 Intriguingly, some CpG-ODNs have been reported to alter cell fate.
95 Initial studies have shown that CpG-1826 modulates osteoclastogenesis
96 through TLR9 (Zou et al., 2003; Amcheslavsky et al., 2005). CpG-KSK13
97 displayed an inhibitory effect on osteoclast differentiation by downregulating
98 TREM-2 (Chang et al., 2009). CpG-2006 and its variants interfere with
99 osteoblast differentiation from mesenchymal stem cells (MSCs) by inhibiting
100 the BMP-Smad signal in a TLR9-independent manner (Norgaard et al., 2010).
101 By contrast, MT01, a 27-base C-rich iODN (Yang et al., 2010), stimulates the
102 differentiation of MSCs into osteoblasts via the ERK-p38 pathway (Feng et
103 al., 2011; Shen et al., 2012; Hou et al., 2012).

104 These findings prompted us to explore a novel ODN that regulates
105 myoblast differentiation. We recently constructed 18-base ODN candidates
106 designed from the genome sequence of a lactic acid bacteria strain,
107 *Lactobacillus rhamnosus* GG (LGG) (Nigar et al., 2017). These synthetic
108 phosphorothioated (PS)-ODNs resistant to nucleases were applied to
109 myoblasts to validate their myogenetic effects. Herein, we report a series of
110 18-base telomeric PS-ODNs, named myogenetic ODNs (myoDNs), that
111 promote myoblast differentiation depending on their conformation but
112 independent of TLR signal. This study presents an innovative approach to
113 regulate cell fate using bacterial-derived ODNs.
114

Materials and Methods

ODNs and Chemicals

The sequences of the ODNs used in this study are described in Supplementary Table S1. PS-ODNs, 6-carboxyfluorescein (6-FAM)-conjugated PS-ODNs, and biotin-conjugated PS-ODNs were synthesized and purified via HPLC (GeneDesign, Osaka, Japan). AS1411 having a phosphodiester backbone was synthesized and desalted (Integrated DNA Technologies, Coralville, IA, USA) as previously reported (Girvan et al., 2006). PS-ODNs, AS1411, berberine hydrochloride (Nacalai, Osaka, Japan), palmatine chloride hydrate (Nacalai), coptisine chloride (Wako, Osaka, Japan), and jatrorrhizine (Wako) were dissolved in endotoxin-free water. An equal volume of endotoxin-free water instead of PS-ODNs and berberine analogs served as negative controls.

Cell Culture

All cells were cultured at 37°C under 5% CO_2 throughout the experiments.

Murine myoblasts (mMBs) were isolated from the skeletal muscle of 4-week-old C57BL/6J mice (Clea Japan, Tokyo, Japan) and primary-cultured as previously described (Takaya et al., 2017; Nihashi et al., 2019b). mMBs were maintained on the dishes or plates coated with collagen type I-C (Cellmatrix; Nitta Gelatin, Osaka, Japan), and cultured in growth medium (GM) for mMB consisting of Ham's F10 medium (Thermo Fisher Scientific,

MA, USA), 20% fetal bovine serum (FBS) (HyClone; GE Healthcare, UT, USA), 2 ng/ml recombinant human basic fibroblast growth factor (Wako), and a mixture of 100 units/ml penicillin and 100 µg/ml streptomycin (PS) (Nacalai).

Primary-cultured human myoblast (hMB) stock of adult healthy female (CC-2580; Lonza, MD, USA) was maintained according to the manufacturer's instruction. hMBs were seeded on collagen-coated dishes, cultured in Skeletal Muscle Growth Media-2 (CC-3245; Lonza) as GM for hMB, and differentiation was induced in differentiation medium (DM) for hMB consisting of DMEM (Nacalai) with 2% horse serum (HS) (HyClone; GE Healthcare) and PS.

C2C12 cells (DS Pharma Biomedical, Osaka, Japan) were seeded on collagen-coated dishes, cultured in GM for C2C12 cells consisting of DMEM with 10% FBS and PS, and induced differentiation in DM for C2C12 cells consisting of DMEM with 2% HS and PS.

Murine embryonic fibroblasts (MEFs) were prepared from E12 embryos of Slc:ICR mice (Japan SLC, Shizuoka, Japan). The embryos that were removed their heads and internal organs were minced in GM for MEFs consisting of DMEM with 10% FBS and PS. The tissue clusters were seeded and cultured for 3 days. Then outgrown cells were dissociated to single cells as MEFs using 0.25% trypsin with 1 mM EDTA (Wako).

MC3T3-E1 cells (RCB1126) were provided by RIKEN BRC (Tsukuba, Japan) through the Project for Realization of Regenerative Medicine and the National Bio-Resource Project of the MEXT, Japan. The cells were maintained in EMEM (Wako) with 10% FBS and PS.

Immunocytochemistry

Immunocytochemistry of myoblasts was performed as previously described (Takaya et al., 2017; Nihashi et al., 2019a; Nihashi et al., 2019b). The myoblasts were fixed with 2% paraformaldehyde, permeabilized with 0.2% Triton X-100, and immunostained with 0.5 μg/ml mouse monoclonal anti- myosin heavy chain (MHC) antibody (MF20; R&D Systems, MN, USA) and 1.0 μg/ml rabbit polyclonal anti-nucleolin antibody (ab22758; Abcam, Cambridge, UK). 0.1 μg/ml each of Alexa Fluor 488-conjugated donkey polyclonal anti-mouse IgG antibody and Alexa Fluor 594-conjugated donkey polyclonal anti-rabbit IgG antibody (Jackson ImmunoResearch, PA, USA) were used as secondary antibodies. Cell nuclei were stained with DAPI (Nacalai). High-resolution fluorescent images were taken under an EVOS FL Auto microscope (AMAFD1000; Thermo Fisher Scientific). The ratio of MHC^+ cells was defined as the number of nuclei in the MHC^+ cells divided by the total number of nuclei, and the fusion index was defined as the number of nuclei in the multinuclear MHC^+ myotubes divided by the total number of nuclei using ImageJ software (National Institutes of Health, USA).

Screening System

1.0×10^4 mMBs or 5.0×10^3 hMBs in 100 μl GM/well were seeded on collagen-coated 96-well plates. The next day, the medium was replaced with GM for mMB or DM for hMB containing PS-ODNs. After 48 h, the mMBs or hMBs were subjected to MHC and DAPI staining. Fluorescent images were

187 automatically captured using CellInsight NXT (Thermo Fisher Scientific).
188 The ratio of MHC^+ cells of mMBs and MHC signal intensities of hMBs were
189 automatically measured using HCS Studio: Cellomics Scan software (Thermo
190 Fisher Scientific). The average value of three wells (4 fields/well) served as
191 the mean of each sample.
192
193 *Cell Counting*
194 5.0×10^4 mMBs/well were seeded on collagen-coated 24-well plates and
195 5.0×10^4 MEFs/well were seeded on 12-well plates. The next day, the medium
196 was replaced with medium containing 1 or 3 μM iSN04. The cells were
197 continuously cultured until cell counting. For counting, the cells were
198 completely dissociated using 0.25% trypsin with 1 mM EDTA and the number
199 of cells was counted using a hemocytometer.
200
201 *Quantitative real-time RT-PCR (qPCR)*
202 2.5×10^5 hMBs in GM were seeded on collagen-coated 60-mm dishes.
203 The next day, the medium was replaced with DM containing 30 μM iSN04.
204 After 24 h, total RNA of the hMBs was isolated using NucleoSpin RNA Plus
205 (Macherey-Nagel, Düren, Germany) and was reverse transcribed using
206 ReverTra Ace qPCR RT Master Mix (TOYOBO, Osaka, Japan). qPCR was
207 performed using GoTaq qPCR Master Mix (Promega, WI, USA) with StepOne
208 Real-Time PCR System (Thermo Fisher Scientific). The amount of each
209 transcript was normalized to that of tyrosine 3-monooxygenase/tryptophan 5-
210 monooxygenase activation protein zeta gene (*YWHAZ*). The results are

presented as fold-change. Primer sequences are listed in Supplementary Table S2.

RNA sequencing (RNA-seq)

The total RNA of hMBs used for qPCR was subjected to RNA-seq (Novogene, Beijing, China). RNA quality was checked using an Agilent 2100 Bioanalyzer (Agilent Technologies, Waldbronn, Germany). RNA integrity number (RIN) values were 10.0 (max score) in all samples (Supplementary Figure S4A). The RNA was subjected to library preparation using Illumina TruSeq RNA and DNA Sample Prep Kits (Illumina, CA, USA). Library quality was confirmed using a Qubit 2.0 fluorometer (Life Technologies; Thermo Fisher Scientific) and Agilent 2100 Bioanalyzer. RNA-seq was performed using Illumina NovaSeq 6000 (Illumina) to generate > 6-GB raw data per sample. Raw data were recorded in FASTQ format. The quality of the read was calculated as the arithmetic mean of the Phred quality score. The reads with following characteristics were discarded: adapter contamination, when uncertain nucleotides constituted > 10% of either read, or when low quality nucleotides (base quality < 20) constituted > 50% of the read. The cleaned reads were mapped to a human reference genome (GRCh38.82) using TopHat2. The number of the reads and mapping efficiencies are summarized in Supplementary Table S3. Expression levels of the transcripts were calculated as fragments per kilobase per million reads (FPKM) values using HTSeq. False discovery rate (FDR) was employed to correct their p values.

Heatmap

Heatmaps of FPKM values were generated via Heatmapper (http://www.heatmapper.ca/) (Babicki et al., 2016) with the following settings: Clustering method, Average linkage; Distance measurement method, Pearson.

Gene Ontology (GO) Analysis

The iSN04-dependent differentially expressed genes (DEGs) were subjected to GO analysis using DAVID Bioinformatics Resources 6.8 (https://david.ncifcrf.gov/) (Huang et al., 2009). The GO terms in biological processes and the KEGG pathways with p values < 0.005 and < 0.05, respectively, were defined as significantly enriched gene clusters. Scatter plots of the DEGs were visualized using R software (R Development Core Team) with a Bioconductor package, Reactome Pathway Analysis (Yu and He, 2015).

STRING Analysis

Functional and physiological interactions of the iSN04-dependent DEGs were visualized using STRING version 11.0 (https://string-db.org/) (Szklarczyk et al., 2019).

Basic Local Alignment Search Tool (BLAST) Search

Homologous sequences of iSN04 in the genomes of humans (taxid: 9605) and mice (taxid: 10088) were searched and scored using BLAST (https://blast.ncbi.nlm.nih.gov/Blast.cgi).

259

260 ***Trivial Trajectory Parallelization of Multicanonical Molecular Dynamics***
261 ***(TTP-McMD)***

262 Starting with the simulation of a single-chain iSN04 structure built
263 from its DNA sequence by NAB in AmberTools (Macke and Case, 1998),
264 enhanced ensemble method, TTP-McMD (Ikebe et al., 2011) was conducted,
265 to sample the equilibrated conformations at 310 K. In the TTP-McMD, the
266 energy range of the multicanonical ensemble covered a temperature range
267 from 280 K to 380 K. Sixty trajectories were used and the production run was
268 conducted for 40 ns in each trajectory (total 2.4 μs). Throughout the
269 simulation, the force field of amber ff12SB (Maier et al., 2015) was used for
270 iSN04, whereas the solvation effect was considered as a generalized-born
271 model (Tsui and Case, 2001). The force field for the berberine molecule was
272 constructed from the RESP charge assigned by the quantum mechanics result
273 of the DFT method with B3-LYP/6-31G*, and the other parameters were
274 taken from GAFF (Wang et al., 2004). In the initial structure of the iSN04-
275 berberine system, a berberine molecule were put at a distance of 40 Å from
276 iSN04. The conformation of the iSN04-berberine complex was calculated via
277 TTP-McMD under the same conditions as the iSN04 simulation.

278

279 ***Agarose Gel Electrophoresis***

280 0.8 nmol PS-ODNs and 0.8 nmol berberine analogs were mixed in 16
281 μl Ham's F10 medium (Supplementary Table S4). In the experiments shown
282 in Supplementary Figure S5B, iSN04 and berberine were mixed in sterile

water, or 4.5 mM of HCl, NaCl, $MgCl_2$, KCl, $CaCl_2$, or $MnCl_2$ solution, or 0.45 mM of $FeSO_4$, $CuSO_4$, or $ZnSO_4$ solution. The mixtures were placed at 4°C overnight, and then subjected to agarose gel electrophoresis using a TAE-buffered 3% agarose gel with 0.5 µg/ml ethidium bromide (EtBr). For colored images, the gels were illuminated by 302 nm ultraviolet (UV) using a UV Transilluminator (UVP, CA, USA) and the images were captured by a digital still camera without any filters. For monochromatic images, the gels were illuminated by 365-nm UV and the images were taken using ImageQuant LAS 500 with an emission bandpass filter of 560 nm (GE Healthcare).

Protein Precipitation, SDS-PAGE, and CBB Staining.

Soluble whole-cell lysates of C2C12 and MC3T3-E1 cells were prepared using lysis buffer consisting of 0.1 M Tris-HCl (pH7.4), 75 mM NaCl, and 1% Triton X-100 (Nacalai) with protease inhibitor cocktail (1 mM 4-(2-aminoethyl)benzenesulfonyl fluoride hydrochloride, 0.8 µM aprotinin, 15 µM E-64, 20 µM leupeptin hemisulfate monohydrate, 50 µM bestatin, and 10 µM pepstatin A) (Nacalai). The biotin-conjugated PS-ODNs were immobilized on streptavidin-coated magnetic beads (Magnosphere MS300/Streptavidin; JSR Life Sciences, CA, USA) according to the manufacturer's instruction. 100 µg of lysates and 0.6 mg of iSN14-beads were mixed in 1 ml lysis buffer with 1% NP-40 (Nacalai), and then gently rotated at 4°C overnight to eliminate the non-specific proteins absorbing onto ODNs or beads. After magnetic pull-down of iSN14-beads, the supernatants were admixed with iSN04-beads and rotated at 4°C overnight. The proteins precipitated by iSN04-beads were

dissociated in lysis buffer with 1% NP-40, 10% glycerol, 2% sodium dodecyl sulfate (SDS) at 95°C for 5 min. The supernatants were subjected to SDS-PAGE using an 8% polyacrylamide gel. The gel was subjected to CBB staining using CBB Stain One Super (Nacalai) and scanned using ImageQuant LAS 500.

Mass Spectrometry

The proteins within the CBB-stained gel were identified by mass spectrometry (MS Bioworks, MI, USA). In-gel digestion was performed using the ProGest robot (Digilab, MA, USA). The gels were washed with 25 mM ammonium bicarbonate followed by acetonitrile, reduced with 10 mM dithiothreitol at 60°C followed by alkylation with 50 mM iodoacetamide at room temperature, digested with trypsin (Promega) at 37°C for 4 h, and quenched with formic acid. Then the supernatant was subjected to analysis by nano LC-MS/MS with a Waters NanoAcquity HPLC system interfaced to a Thermo Fisher Q Exactive. Peptides were loaded on a trapping column and eluted over a 75-µm analytical column at 350 nl/min. Both columns were packed with Luna C18 resin (Phenomenex, CA, USA). The mass spectrometer was operated in data-dependent mode, with the Orbitrap operating at 70,000 FWHM and 17,500 FWHM for MS and MS/MS, respectively. The 15 most abundant ions were selected for MS/MS analysis. Data were searched using a local copy of Mascot with the following parameters: Enzyme, trypsin/P; Database, SwissProt Mouse; Fixed modification, carbamidomethyl; Variable modifications, oxidation, acetyl, pyro-Glu, deamidation; Mass values,

monoisotopic; Peptide mass tolerance, 10 ppm; Fragment mass tolerance, 0.02 Da; Max missed cleavages, 2. Mascot DAT files were parsed into Scaffold (Proteome Software, OR, USA) for validation, filtering, and to create a non-redundant list per sample. Data were filtered using 1% protein and peptide FDR, which required at least two unique peptides per protein.

Western Blotting

Soluble whole-cell lysates of the hMBs treated with 30 μM of iSN04 or AS1411 in DM for 48 h were prepared as described above. The lysates were denatured with 50 mM Tris-HCl, 10% glycerol, and 2% SDS at 95°C for 5 min. 10 μg of protein samples were subjected to SDS-PAGE on a 10% polyacrylamide gel followed by Western blotting using an iBlot 2 Dry Blotting System (Thermo Fisher Scientific). 1.0 μg/ml each of rabbit polyclonal anti-nucleolin antibody, mouse monoclonal anti-p53 antibody (PAb 240; Abcam), and mouse monoclonal anti-glyceraldehyde 3-phosphate dehydrogenase (GAPDH) antibody (5A12; Wako) were used as primary antibodies. 0.1 μg/ml each of horseradish peroxidase (HRP)-conjugated goat anti-rabbit and anti-mouse IgG antibodies (Jackson ImmunoResearch) were used as secondary antibodies, respectively. HRP activity was detected using ECL Prime reagents and ImageQuant LAS 500. The quantities of nucleolin and p53 proteins were normalized to that of GAPDH using ImageJ software.

Statistical Analyses

354 Results are presented as the mean ± standard error. Statistical
355 comparisons were performed using unpaired two-tailed Student's t test,
356 multiple comparison test with Dunnett's test, Tukey-Kramer test, Scheffe's F
357 test, or Williams' test where appropriate following one-way analysis of
358 variance using R software. Statistical significance was set to $p < 0.05$.
359

Results

Identification of myoDNs

Fifty 18-base PS-ODNs (iSN01-iSN50) (Supplementary Table S1) derived from the LGG genome were subjected to a screening system to investigate the effects on myogenic differentiation of primary-cultured mMBs. 10 μM PS-ODNs were administered to the mMBs maintained in GM for 48 h. The mMBs were immunostained for MHC, a terminal differentiation marker of skeletal muscle (Supplementary Figure S1). The percentages of MHC^+ cells were automatically quantified in a non-biased manner. As shown in Figure 1A, seven PS-ODNs (iSN01-iSN07) significantly increased the ratio of MHC^+ cells, but other PS-ODNs did not alter the differentiation of mMBs. iSN01-iSN07 reproducibly induced myogenic differentiation of another independently isolated lot of mMBs (Supplementary Figure S2A), regardless of variation in the basal differentiation efficiency. In both screening results, iSN04' exhibited the highest myogenetic activity (Figure 1A and Supplementary Figure S2A). These experiments were performed using iSN04' (AAG TTA GGG TGA GGG TGA; not existing in LGG genome) instead of iSN04 (AGA TTA GGG TGA GGG TGA; existing in LGG genome). As the activities of iSN04' and iSN04 were completely equal (Supplementary Figure S2C), iSN04 was utilized in the following experiments. iSN04 also promoted myogenic differentiation of the murine myoblast cell line C2C12 (Supplementary Figure S2D) and primary-cultured hMBs (Figure 1B). The

ratio of MHC$^+$ myocytes and fused myotubes was significantly increased by iSN04 in myoblasts in both mice and humans.

In stem cells or their progenies, proliferation and differentiation are inverse processes, which negatively regulate each other (Ruijtenberg and van den Heuvel, 2016). The number of mMBs treated with iSN01-iSN07 was significantly lower than that of the control (Supplementary Figure S2B), indicating that iSN01-iSN07 inhibits myoblast proliferation. Continuous cell counting revealed that iSN04 suppressed the growth of mMBs in a dose-dependent manner; however, iSN04 did not alter the number of MEFs (Figure 1C). This demonstrates that the reduction in cell numbers in the iSN04-treated myoblasts was due to enhanced myogenic differentiation. qPCR revealed that iSN04 significantly upregulated the levels of myogenic transcription factors MyoD (*MYOD1*) and myogenin (*MYOG*), resulting in marked induction of embryonic MHC (*MYH3*) in hMBs (Figure 1D). In contrast, iSN04 did not alter the levels of undifferentiated myoblast markers, Pax7 (*PAX7*) and Myf5 (*MYF5*). These data show that iSN04 inherently promotes myoblast differentiation by activating the myogenic gene expression program.

We designated iSN01-iSN07 as "myoDNs", denoting myogenetic ODNs. They are a novel type of ODNs that induce myoblast differentiation.

myoDN Activity Is Independent of TLR Signaling

iSN01-iSN07 share a tandem repeat of a telomeric hexamer (TTAGGG TGAGGG) (Supplementary Figure S2E). A previous study has

reported that a 24-base telomeric iODN (Tel-ODN) (Supplementary Table S1) suppresses human B-cell activation depending on TLR3, TLR7, and TLR9 (Sackesen et al., 2013). We have indicated that a 17-base telomeric iODN (iSG3; CCTCA TTAGGG TGAGGG) inhibits CpG-ODN (MsST)-induced interleukin (IL)-6 expression through intracellular incorporation in murine macrophages (Wang et al., 2015). Administration of 6-FAM-conjugated iSN04 to hMBs also showed that iSN04 was internalized into the cytoplasm within 2 h (Figure 1E). Contrarily, we have already confirmed that iSN01-iSN07 does not affect MsST-induced IL-6 expression in murine splenocytes (Nigar et al., 2017), suggesting that myoDNs are not iODNs. RT-PCR revealed that hMBs, mMBs, and C2C12 cells expressed all TLR genes except for *Tlr12* in C2C12 cells (Supplementary Figures S3A and S3B). To investigate the dependency of myoDN activity on TLR signaling, hMBs were treated with iSN04, Tel-ODN, or CpG-2006 (Supplementary Table S1). CpG-2006 is the TLR9 ligand initiating inflammatory responses in human lymphocytes and murine macrophages (Pohar et al., 2015). In the absence of iSN04, neither CpG-2006 nor Tel-ODN induced the differentiation of hMBs into MHC^+ myocytes (Figure 1F). In the presence of iSN04, neither CpG-2006 nor Tel-ODN inhibited iSN04-induced myogenic differentiation. RNA-seq data (see next section) showed that transcription levels of the genes involved in the TLR signaling pathway were not altered in the iSN04-treated hMBs (Supplementary Figure S3C). These results demonstrate that iSN04 is not a TLR ligand, dissimilar to immunogenic CpG-ODNs and iODNs. It is assumed

that myoDN activity inducing myogenic differentiation is independent of TLR signaling.

Profile of iSN04-Dependent Gene Expression

We comprehensively surveyed the iSN04-dependent gene expression profile of hMBs. Total RNA of the hMBs treated with 30 μM iSN04 in DM for 24 h was subjected to RNA-seq (Supplementary Figure S4A). 51.3 million reads per sample were acquired, of which approximately 45.9 million reads (90.0%) were mapped to a human reference genome (Supplementary Table S3). In total, 60,448 transcripts were identified and their expression levels were calculated as FPKM. FPKM values of myogenic genes exhibited a pattern compatible with qPCR results; iSN04 significantly downregulated *MYF5* and upregulated *MYOD1* and *MYOG* (Supplementary Figure S4B). A total of 22,269 transcripts showed significant expression levels (FPKM > 0.1) in the control or iSN04 group. Of them, 899 transcripts were differentially expressed (> 1.5-fold) with the significance of FDR $p < 0.05$ (Supplementary Data). Of which 476 and 423 transcripts were upregulated and downregulated by iSN04, respectively. These DEGs depending on iSN04 were subjected to GO analysis. The 476 iSN04-upregulated DEGs significantly formed multiple gene clusters for muscle adaptation, contraction, and formation, which abundantly included sarcomeric components (myosin, actin, troponin, and their associated proteins) and transcription factors (myogenin, Hes1, Smad7, and Wnt10a) (Figure 2A). In contrast, the 423 iSN04-downregulated DEGs involved many clusters related to cell cycle and

proliferation with higher significance (Figure 2B). These expression profiles of the iSN04-dependent DEGs corresponded well with the phenotype of iSN04-treated myoblasts, which showed promoted myogenic differentiation and arrested cell growth. STRING analysis visualized functional and physiological interactions of the DEGs or their products (Figure 2C). The tightly connected networks were detected in both DEG groups. Especially within the iSN04-downregulated group, 173 of the 423 DEGs (40.9%) were concentrated in the primary cluster, suggesting that iSN04 possibly suppresses at least one of the major nodes of the transcriptome at the early stage regulating myoblast fate. These data indicate that iSN04 globally modulates gene expression by orchestrating the myogenic program and cell cycle in myoblasts.

myoDN Activity Is Dependent on Its Structure

ODNs are classified into three categories according to their mechanism of action: antisense nucleotides, aptamers, and immunogenic ODNs as TLR ligands. myoDN activity was independent of TLR signals. Furthermore, immunogenic ODNs are often species-specific (Pohar et al., 2015), but iSN04 induces the differentiation of both murine and human myoblasts. To investigate the potential of myoDNs as antisense ODNs, the homologous sequences of iSN04 in human and murine genomes were surveyed using BLAST. The BLAST results displayed 59 loci in humans and 39 loci in mice that had iSN04-homologous sequences. However, there was no common gene or locus between humans and mice, denying that iSN04 serves

as an antisense nucleotide. Intriguingly, the heat-denatured iSN02 lost the ability to induce myoblast differentiation (Supplementary Figure S2F), which strongly suggests that myoDN activity arises from its structure. Notably, iSN04 was resistant to thermal denaturation (Supplementary Figure S2G). The iSN04 conformation is considered to be relatively stable and can recover from denaturation in a short period. This might also be the reason why iSN04 presented the highest activity among the myoDNs.

The conformational properties of iSN04 under water conditions were computationally investigated using TTP-McMD (Ikebe et al., 2011). iSN04 at 310 K showed a compact globular structure (average radius: 0.96 nm), not a linear strand (Figure 3A). iSN04 displayed varied conformations, but their variations seemed to be limited within a certain range (Supplementary Movie). For fine conformation analysis, the contact probabilities between the residues of iSN04 were calculated. The ensemble-averaged contact probabilities at 310 K over all the simulated iSN04 structures were rendered as a contact map (Figure 3B). Three guanines at the 13-15th bases stacked upon each other, suggesting that this $G_{13\text{-}15}$ stack is the stable center of the iSN04 structure. The impact of the $G_{13\text{-}15}$ bases on iSN04 activity was examined using mutant iSN04. A series of deletions in the $G_{13\text{-}15}$ bases gradually attenuated the myogenetic activity of iSN04. In particular, $iSN04^{\Delta 13\text{-}15}$ completely lost its activity (Figure 3G), demonstrating that the $G_{13\text{-}15}$ stack is indispensable for iSN04 activity.

Berberine Enhances iSN04 Activity

We hypothesized that stabilization of the $G_{13\text{-}15}$ stack would improve iSN04 activity. Telomeric DNA is known to form a highly ordered conformation. The G-quartet is a square aromatic surface constructed by the four guanines interacting with its neighbors via two hydrogen bonds. G-quartets stack upon each other to build the four-stranded G-quadruplex (Ou et al., 2008). Berberine, an isoquinoline alkaloid (Supplementary Figure S5A), interacts with the G-quartet and stabilizes the G-quadruplex structure derived from human telomeric DNA (Bazzicalupi et al., 2012). We tested whether iSN04 physically interacts with berberine. Briefly, iSN04 and berberine were mixed in F10 medium (Supplementary Table S4), subjected to electrophoresis, and stained with EtBr, which fluoresces red at 620 nm. The iSN04-berberine complex can be imaged with yellow fluorescence because berberine fluoresces green at 530 nm (Guo et al., 2015; Shinji et al., 2020). Indeed, yellow emissions of the iSN04-berberine complex were detected at a slightly higher molecular weight compared to iSN04 alone (Figure 3E). Not only iSN04 but also all other myoDNs interacted with berberine (Supplementary Figure S5C). G-quartets generally coordinate cations (Ou et al., 2008), and berberine binds to the telomeric DNA holding K^+ (Bazzicalupi et al., 2012). We examined the requirement of cations for the iSN04-berberine complex using cationic solutions. Ca^{2+} was found to be necessary for the iSN04-berberine complex (Supplementary Figure S5B). Moreover, Mg^{2+} facilitated the interaction between iSN04 and berberine, but its effect was markedly weaker than that of Ca^{2+}. These results suggest that berberine

525 binds to the G-quartet- or G-quadruplex-like structure within iSN04, which
526 is probably formed by the $G_{13\text{-}15}$ stack.

527 Administration of iSN04 and berberine to mMBs proved that the
528 activity of the iSN04-berberine complex was significantly higher than that of
529 single iSN04 (Figure 3F). As berberine alone did not alter myoblast
530 differentiation, it is possible that the improved activity of the iSN04-
531 berberine complex is not a synergistic effect. Berberine is speculated to
532 enhance the inherent activity of iSN04 by stabilizing or shifting the
533 conformation. In some cases, one G-quartet binds to two berberine molecules
534 (Bazzicalupi et al., 2012). To optimize the molar ratio of iSN04 to berberine,
535 mMBs were treated with 0-3 μM iSN04 and 0-30 μM berberine. iSN04
536 exhibited the highest myogenetic activity when mMBs were co-treated with
537 an equal molar of berberine (Figure 3H). Conformation of the iSN04-
538 berberine complex at a molar ratio of 1:1 was simulated using TTP-McMD.
539 Berberine interacted exactly with the $G_{13\text{-}15}$ stack of iSN04 (Figure 3C).
540 Deletions of the $G_{13\text{-}15}$ bases of iSN04 experimentally demonstrated that
541 berberine actually interacts with these guanines (Figure 3I, upper panel). The
542 contact map of the iSN04-berberine complex showed that the $G_{7\text{-}9}$ bases are
543 stacked in addition to the $G_{13\text{-}15}$ stack (Figure 3D). Berberine also contacted
544 the G_9 and consequently, it fits into the pocket assembled from the $G_{7\text{-}9}$ and
545 $G_{13\text{-}15}$ stacks. iSN04 has two telomeric hexamers; TTAGGG and TGAGGG. We
546 investigated the influence of the T_5 and G_{11} of iSN04 on myogenetic activity
547 and berberine binding. Both the T5G and G11T substitutions did not affect
548 iSN04 activity (Figure 3G). However, the T5G substitution interfered with

549 the formation of iSN04-berberine complex, and iSN04^{G11T} interacted with
550 berberine as well as intact iSN04 (Figure 3I, lower panel). The contact maps
551 indicated that the T_5 relatively remains at a distance from other bases. On
552 the contrary, guanines tend to interact with other bases. The extra guanine
553 inserted by the T5G substitution might have perturbed the pocket required
554 for iSN04 to bind to berberine.

555 We further examined the iSN04-enhancing abilities of three berberine
556 analogs, coptisine, palmatine, and jatrorrhizine (Supplementary Figure S5A).
557 Coptisine and berberine formed a complex with iSN04. Palmatine weakly
558 interacted with iSN04, but jatrorrhizine did not interact at all (Figure 3J).
559 Correspondingly, coptisine significantly improved the myogenetic activity of
560 iSN04 to the same level as the iSN04-berberine complex (Figure 3K). These
561 results illustrate that the 2,3-methylenedioxy ring of the berberine backbone
562 is important for interacting with iSN04.

563

564 ***iSN04 Targets Nucleolin and Increases p53 Protein***

565 The structure-dependent myogenetic activity of iSN04 suggests the
566 presence of iSN04-target proteins. We surveyed iSN04-binding proteins by
567 precipitation assay. Biotin-conjugated iSN04 was immobilized on
568 streptavidin-beads at the 5' or 3' end (iSN04-5'-Bio and iSN04-3'-Bio,
569 respectively). Soluble whole-cell lysates were pre-pulled-down with iSN14-
570 beads to eliminate the absorption of non-specific proteins onto ODNs or beads.
571 After removing off-target proteins, the lysates were precipitated with iSN04-
572 beads, followed to SDS-PAGE and CBB staining. Surprisingly, iSN04-binding

573 protein was not detected in C2C12 cell lysates (data not shown). Next, the
574 lysate of the murine osteoblast cell line MC3T3-E1 was prepared because
575 iSN04 affected MC3T3-E1 differentiation (unpublished data). Both iSN04-5'-
576 Bio and iSN04-3'-Bio precipitated the identical single protein with an
577 expected size of 112 kDa, which was not precipitated by iSN14-beads or beads
578 alone (Figure 4A). Mass spectrometry identified the iSN04-binding protein as
579 nucleolin (Supplementary Tables S5 and S6). Although the molecular weight
580 of nucleolin is 77 kDa, it is practically detected at 100-110 kDa because of the
581 acidic amino acids in the N-terminal domain (Jia et al., 2017). Nucleolin is a
582 multifunctional phosphoprotein located in the nucleolus, cytoplasm, and
583 plasma membrane depending on the context of cellular processes such as gene
584 expression, protein shuttling, cytokinesis, and apoptosis. Expression and
585 subcellular localization of nucleolin are frequently abnormal in rapidly
586 growing cells, typically cancers (Jia et al., 2017). A recent study reported that
587 the amount and localization of nucleolin is involved in myogenic
588 differentiation of C2C12 cells (Tang et al., 2017), but its precise mechanism
589 is still unknown.

590 A 26-base G-rich non-immunogenic ODN, AS1411 (Supplementary
591 Table S1), is an established anti-nucleolin aptamer which has been utilized
592 in several clinical trials on cancers (Bates et al., 2009; Yazdian-Robati et al.,
593 2019). AS1411 promoted myogenic differentiation of hMBs to the same extent
594 as iSN04 (Figure 4B), proving that iSN04 targets nucleolin in myoblasts.
595 Immunostaining revealed that nucleolin initially localized in the nucleoli of
596 hMBs and C2C12 cells in their undifferentiated states. Nucleolin was then

translocated into the cytoplasm of MHC$^+$ myotubes throughout myogenic differentiation (Figure 4C and Supplementary Figure S6A) as previously reported (Tang et al., 2017). The mRNA levels of nucleolin (*NCL*) in hMBs were increased during differentiation but did not chang after iSN04 treatment (Supplementary Figures S6C and S6D). In addition, nucleolin localization in hMBs or C2C12 cells was not shifted by iSN04 or AS1411 (Figure 4D and Supplementary Figure S6B). These results correspond to those of previous studies, which confirmed that AS1411 does not alter nucleolin localization in cancer cells (Litchfield et al., 2012; Reyes-Reyes et al., 2015; Ramos et al., 2020). Nucleolin has been reported to target the untranslated region (UTR) of p53 mRNA to interfere with its translation in tumor cells (Takagi et al., 2005; Chen et al., 2012). Nucleolin inhibition by AS1411 increases p53 protein levels and suppresses cell proliferation in glioma cells (Cheng et al., 2016). As p53 induces myogenic differentiation (Cerone et al., 2000; Porrello et al., 2000), antagonizing nucleolin in myoblasts by iSN04 or AS1411 was assumed to upregulate p53 protein and promote differentiation. RNA-seq data showed that the iSN04-dependent DEGs were enriched in the p53 signaling pathway (Figure 4E and Supplementary Figure S6E). Western blotting showed that both iSN04 and AS1411 increased p53 protein levels in hMBs (Figure 4F), even though iSN04 decreased the mRNA level of p53 (*TP53*) (Supplementary Figure S6F).

These data demonstrate that iSN04 antagonizes nucleolin to recover the suppressed p53 translation. The iSN04-increased p53 protein level activates downstream signal to arrest the cell cycle and induce myoblast

621 differentiation. The results of this study present evidence that bacterial-
622 derived ODNs can serve as aptamers to modulate cell fate.
623

Discussion

To our knowledge, this is the first report of the ODNs promoting myogenic differentiation of skeletal muscle myoblasts. myoDNs are 18-base telomeric ODNs designed from the LGG genome sequence. Such bacterial ODNs serve as immunogenic ODNs recognized by TLRs and modulate the innate immune system (Krieg et al., 1995; Klinman, 2008). Among them, telomeric ODNs, also termed iODNs, are known to suppress inflammatory responses (Sackesen et al., 2013; Wang et al., 2015). In our previous study, myoDNs (iSN01-iSN07) were not iODNs (Nigar et al., 2017). iSN04, the myoDN presenting the highest activity, induced myoblast differentiation independent of TLR signaling. myoDNs are thus defined as a novel type of ODN that regulates cell fate through a unique mechanism. A previous study reported that CpG-2006 interferes with the osteoblastic differentiation of MSCs in a TLR9-independent manner, but its direct target is unknown (Norgaard et al., 2010). CpG-2006 was originally identified as a TLR9 ligand that activates immune responses (Hartmann et al., 2000; Bauer et al., 2001). The dual role of CpG-2006, in addition to myoDNs, implies that other bacterial ODNs might also exert non-immunological functions.

The present study revealed that the myogenetic activity of iSN04 arises from its conformation rather than its sequence. Molecular simulation and a series of mutant iSN04 demonstrated that the $G_{13\text{-}15}$ stack within the second telomeric hexamer is essential for iSN04 activity. It is also indicated that berberine physically interacts with iSN04 via the $G_{13\text{-}15}$ stack and

enhances the myogenetic ability of iSN04, probably by stabilizing or optimizing the structure. This is the initial instance of functional improvement of ODNs by small molecules. Berberine is a safe isoquinoline alkaloid isolated from medicinal plants, that exhibits various bioactivities and has been utilized in clinical studies on diabetes, osteoporosis, and cancer (Imenshahidi and Hosseinzadeh, 2019). Berberine has also been studied as a ligand of the G-quadruplex, which is often formed in oncogenic promoter regions and regulates gene expression by recruiting transcriptional machinery (Siddiqui-Jain et al., 2002). Therefore, berberine derivatives that block G-quadruplexes can be potential anti-tumor drugs (Ou et al., 2008; Bazzicalupi et al., 2012). From these points of view, the modification of the structure and function of telomeric ODN by berberine provides a safe and reasonable technique for further research, development, and application of ODNs.

We identified nucleolin as a direct target of iSN04. The established anti-nucleolin aptamer, AS1411, also promoted myoblast differentiation, which proved that iSN04 antagonizes nucleolin. AS1411 has been reported to polymorphically fold into various conformations, including G-quadruplex structures (Dailey et al., 2010; Supplementary Figure S6G). Interestingly, iSN04 but not AS1411 interacted with berberine (Supplementary Figure S5D), and AS1411 but not iSN04 decreased nucleolin levels (Figure 4F), which suggests the presence of subtle structural and functional differences. Experimental determination of the iSN04 structure will provide valuable information on the similarity and dissimilarity between iSN04 and AS1411,

672 which will be useful for building novel aptamers based on their conformations.
673 Aptamers are usually developed via in vitro methodology using a specific
674 target, systemic evolution of ligands by exponential enrichment (SELEX)
675 (Wang et al., 2019). However, AS1411 is a non-SELEX aptamer that was
676 screened as an inhibitor for cancer cell growth (Bates et al., 2009).
677 Precipitation assay and mass spectrometry identified nucleolin as an AS1411
678 target (Girvan et al., 2006). Although AS1411 interacts with at least 15
679 proteins including nucleolin (Girvan et al., 2006), nucleolin has been a
680 primary target of AS1411. Because aptamers usually recognize membrane
681 proteins, and nucleolin is present on the plasma membrane of cancer cells
682 (Bates et al., 2009; Jia et al., 2017; Yazdian-Robati et al., 2019).

683 Unlike many aptamers, iSN04 and AS1411 exert their effects inside
684 myoblasts. iSN04 was spontaneously incorporated into myoblasts. Nucleolin
685 initially localized in the nucleoli of growing myoblasts and diffused into the
686 cytoplasm during myotube formation. However, iSN04 and nucleolin were not
687 observed on the surface of myoblasts throughout differentiation. As discussed
688 below, nuclear nucleolin serves as an mRNA-binding protein that regulates
689 translation (Fahling et al., 2006). These findings indicate that iSN04 and
690 AS1411 conceivably function in the nuclei of myoblasts. In general, single-
691 strand ODNs are efficiently taken into the cytoplasm without carriers
692 through gymnosis. Although its mechanism has not been completely
693 understood, ODNs are considered to be incorporated by endocytosis,
694 transported to the endosome, and are transferred to the cytoplasm through
695 the endosomal membrane, probably due to their lower molecular weights and

higher hydrophobicities compared to double-strand nucleotides. The released ODNs into the cytoplasm can accumulate in the nucleus by associating with chaperones or RNA-binding proteins (Juliano, 2018).

Nucleolin interferes with the translation of p53 mRNA by binding to its UTR (Takagi et al., 2005; Chen et al., 2012). Our study showed that antagonizing nucleolin by iSN04 or AS1411 increased p53 protein levels in myoblasts, as reported in AS1411-treated glioma cells (Cheng et al., 2016). The role of p53 in myoblasts has been intensively studied. An initial study found that the dominant-negative form of p53 inhibits the differentiation of C2C12 cells (Soddu et al., 1996). During myogenic differentiation, p53 cooperates with MyoD (Cerone et al., 2000) to activate transcription of retinoblastoma protein (Porrello et al., 2000), which serves as a cofactor of MyoD to arrest the cell cycle and facilitate muscle cell commitment (Gu et al., 1993; Novitch et al., 1996). A recent study revealed that p53 with MyoD coactivates the expression of the pro-apoptotic protein PUMA (Harford et al., 2017), which is required for the apoptosis associated with myoblast differentiation (Shaltouki et al., 2007; Harford et al., 2010). This accumulating evidence corroborates the findings that iSN04 upregulates p53 protein and induces myoblast differentiation.

Interestingly, iSN04 did not affect the growth of MEFs expressing nucleolin (Supplementary Figure S6H). In the precipitation assays, iSN04 pulled down nucleolin in the lysates of MC3T3-E1 cells but not of C2C12 cells, even though the amounts of nucleolin were nearly equal between the lysates (Supplementary Figure S6I). According to circumstances, nucleolin is post-

720 translationally modified such as phosphorylation and glycosylation (Barel et
721 al., 2001; Losfeld et al., 2009), and interacts with various partners including
722 nucleotides and proteins (Jia et al., 2017). Probably due to that, AS1411
723 precipitates only certain forms of nucleolin (Teng et al., 2007; Bates et al.,
724 2009). The amounts of the iSN04-binding form of nucleolin in C2C12 cells
725 might be less than that in MC3T3-E1 cells and not enough to be detected via
726 CBB staining. It is possible that the mode of existence of nucleolin differs
727 among the cells, which affects its affinity to iSN04.

728 The precise role of nucleolin during myogenic differentiation is still
729 not fully understood. A moderate decline in nucleolin protein by miR-34b has
730 been reported to upregulate myogenic expression (Tang et al., 2017). This
731 study showed that nucleolin levels decreased through differentiation of
732 C2C12 cells; however, our results using primary-cultured hMBs showed
733 increased nucleolin expression upon differentiation. As nucleolin is potently
734 induced in actively proliferating cells like tumors (Jia et al., 2017), nucleolin
735 levels might be high in the immortalized C2C12 cell line. Therefore, nucleolin
736 function in myoblasts needs to be further investigated using primary-cultured
737 cells or in vivo models. In both hMBs and C2C12 cells, nucleolin initially
738 localized in the nucleoli and then diffused into the cytoplasm through
739 differentiation. An analogous shift of nucleolin localization has been observed
740 during adipogenic differentiation of 3T3-L1 pre-adipocytes (Wang et al., 2015).
741 The biological activities of nucleolin can vary depending on its subcellular
742 distribution. Numerous studies have revealed that nucleolar nucleolin
743 regulates RNA metabolism, nucleoplasmic nucleolin modulates gene

744 expression, cytoplasmic nucleolin serves as a shuttle protein, and cell surface
745 nucleolin is involved in various signaling pathways (Jia et al., 2017).
746 Elucidating the relationship between nucleolin localization and
747 differentiation of precursor cells would be important to understand the fine-
748 tuned mechanism of myoDNs.

749 To establish myoDNs as potential drug seeds for muscle diseases,
750 their pharmacological actions need to be investigated in vivo. Intramuscular
751 injection (i.m.) of antisense nucleotides have been clinically applied to treat
752 Duchenne muscular dystrophy (Quemener et al., 2020). However, i.m. is
753 painful and there is a risk of sterile abscess formation, therefore it is not
754 suitable for prevention or treatment of the long-termed muscle atrophy
755 associating with aging or chronic diseases. We have previously developed
756 ODN nanocapsules (ODNcaps) as an oral delivery system of ODNs. Oral
757 administration of the capsuled iODN to atopic model mice successfully
758 suppressed immune responses in dermatitis (Wang et al., 2015). ODNcaps
759 would be also useful to deliver myoDNs to atrophic muscle tissue. Further
760 studies using adequate animal model and drug delivery system are required
761 for clinical application of myoDNs in future.

762

763 **Conclusion**

764 This study presents that bacterial genome-derived myoDNs promote
765 myogenic differentiation by targeting nucleolin. The myoDN activities can be
766 enhanced by conformational changes via binding to berberine. myoDNs are

767 expected to be novel and unique drug candidates for muscle diseases,
768 including atrophy, in which myoblasts are functionally deteriorated.
769

Data Availability Statement

FASTQ raw read data of RNA-seq were deposited in the DDBJ Sequence Read Archive (DRA; Research Organization of Information and Systems, National Institute of Genetics, Mishima, Japan) with the accession number: DRA008498.

Ethics Statement

All experimental procedures were conducted in accordance with the Regulations for Animal Experimentation of Shinshu University, and the animal experimentation protocol was approved by the Committee for Animal Experiments of Shinshu University.

Author Contributions

TT designed the study; TT and KU wrote the manuscript; SS, YN, SN, and TT performed the experiments and data analyses; KU performed molecular simulation and proposed iSN04-berberine interaction; TS designed and provided the ODNs.

Funding

This study was supported in part by Grants-in Aid from the Japan Society for the Promotion of Science (16K19397 and 19K05948), the TOBE MAKI Scholarship Foundation (17-JA-503), the Skylark Food Science Institute, the Takano Science Foundation, and the Japan Society for

Bioscience, Biotechnology, and Agrochemistry to TT, and a Grant-in-Aid from the Fund of Nagano Prefecture to Promote Scientific Activity (H30-3-3) to SS.

Conflict of Interst

Shinshu University has been assigned the invention of myoDNs by TT, KU, and TS, and Japan Patent Application 2018-568609 has been filed on February 15, 2018.

Acknowledgments

C57BL/6J mice and C2C12 cells were kindly provided by Dr. Sachi Tanaka and Dr. Shinichi Yonekura, of Shinshu University. The preprint has been posted on bioRxiv (doi: 10.1101/2020.10.07.330472).

806 **References**

807

808 Amcheslavsky, A., Hemmi, H., Akira, S., and Bar-Shavit, Z. (2005).
809 Differential contribution of osteoclast- and osteoblast-lineage cells to CpG-
810 oligodeoxynucleotide (CpG-ODN) modulation of osteoclastogenesis. *J. Bone*
811 *Miner. Res.* 20, 1692-1699. doi: 10.1359/JBMR.050515

812 Anker, S.D., Ponikowski, P., Varney, S., Chua, T. P., Clark, A. L., Webb-Peploe,
813 K. M., et al. (1997). Wasting as independent risk factor for mortality in
814 chronic heart failure. *Lancet* 349, 1050-1053. doi: 10.1016/s0140-
815 6736(96)07015-8

816 Babicki, S., Arndt, D., Marcu, A., Liang, Y., Grant, J. R., Maciejewski, A., et
817 al. (2016). Heatmapper: web-enabled heat mapping for all. *Nucleic Acids*
818 *Res.* 44, W147-W153. doi: 10.1093/nar/gkw419

819 Barel, M., Le Romancer, M., and Frade, R. (2001). Activation of the EBV/C3d
820 receptor (CR2, CD21) on human B lymphocyte surface triggers tyrosine
821 phosphorylation of the 95-kDa nucleolin and its interaction with
822 phosphatidylinositol 3 kinase. *J. Immunol.* 166, 3167-3173. doi:
823 10.4049/jimmunol.166.5.3167

824 Bates, P. J., Laber, D. A., Miller, D. M., Thomas, S. D., and Trent, J. O. (2009).
825 Discovery and development of the G-rich oligonucleotide AS1411 as a novel
826 treatment for cancer. *Exp. Mol. Pathol.* 86, 151-164. doi:
827 10.1016/j.yexmp.2009.01.004

828 Bauer, S., Kirschning, C. J., Hacker, H., Redecke, V., Hausmann, S., Akira, S.,
829 et al. (2001). Human TLR9 confers responsiveness to bacterial DNA via

species-specific CpG motif recognition. *Proc. Natl. Acad. Sci. USA* 98, 9237-9242. doi: 10.1073/pnas.161293498

Bazzicalupi, C., Ferraroni, M., Bilia, A. R., Scheggi, F., and Gratteri, P. (2012). The crystal structure of human telomeric DNA complexed with berberine: an interesting case of stacked ligand to G-tetrad ratio higher than 1:1. *Nucleic Acids Res.* 41, 632-638. doi: 10.1093/nar/gks1001

Brack, A.S., Conboy, M. J., Roy, S., Lee, M., Kuo, C. J., Keller, C., et al. (2007). Increased Wnt signaling during aging alters muscle stem cell fate and increases fibrosis. *Science* 317, 807-810. doi: 10.1126/science.1144090

Carrero, J. J., Chmielewski, M., Axelsson, J., Snaedal, S., Heimburger, O., Barany, P., et al. (2008). Muscle atrophy, inflammation and clinical outcome in incident and prevalent dialysis patients. *Clin. Nutr.* 27, 557-564. doi: 10.1016/j.clnu.2008.04.007

Cerone, M. A., Marchetti, A., Bossi, G., Blandino, G., Sacchi, A., and Soddu, S. (2000). p53 is involved in the differentiation but not in the differentiation-associated apoptosis of myoblasts. *Cell Death Differ.* 7, 506-508. doi: 10.1038/sj.cdd.4400676

Chang, J. H., Chang, E. J., Kim, H. H., and Kim, S. K. (2009). Enhanced inhibitory effects of a novel CpG motif on osteoclast differentiation via TREM-2 down-regulation. *Biochem. Biophys. Res. Commun.* 389, 28-33. doi: 10.1016/j.bbrc.2009.08.080

Chen, J., Guo, K., and Kastan, M. B. (2012). Interactions of nucleolin and ribosomal protein L26 (RPL26) in translational control of human p53 mRNA. *J. Biol. Chem.* 287, 16467-16476. doi: 10.1074/jbc.M112.349274

854 Chen, Q., Luo, S., Zhang, Y., and Chen, Z. (2011). Development of a liquid
855 chromatography-mass spectrometry method for the determination of
856 ursolic acid in rat plasma and tissue: application to the pharmacokinetic
857 and tissue distribution study. *Anal. Bioanal. Chem.* 399, 2877-2884. doi:
858 10.1007/s00216-011-4651-x
859 Cheng, Y., Zhao, G., Zhang, S., Nigim, F., Zhou, G., Yu, Z., et al. (2016).
860 AS1411-induced growth inhibition of glioma cells by up-regulation of p53
861 and down-regulation of Bcl-2 and Akt1 via nucleolin. *PLoS One* 11,
862 e0167094. doi: 10.1371/journal.pone.0167094
863 Cui, W., Liu, C. X., Zhang, Y. C., Shen, Q., Feng, Z. H., Wang, J., et al. (2019).
864 A novel oleanolic acid derivative HA-19 ameliorates muscle atrophy via
865 promoting protein synthesis and preventing protein degradation. *Toxicol.*
866 *Appl. Pharmacol.* 378, 114625. doi: 10.1016/j.taap.2019.114625
867 Dailey, M. M., Miller, M. C., Bates, P. J., Lane, A. N., and Trent, J. O. (2010).
868 Resolution and characterization of the structural polymorphism of a single
869 quadruplex-forming sequence. *Nucleic Acids Res.* 38, 4877-4888. doi:
870 10.1093/nar/gkq166
871 Dumont, N. A., Bentzinger, C. F., Sincennes, M. C., and Rudnicki, M. A. (2015).
872 Satellite cells and skeletal muscle regeneration. *Compr. Physiol.* 5, 1027-
873 1059. doi: 10.1002/cphy.c140068
874 Fahling, M., Mrowka, R., Steege, A., Nebrich, G., Perlewitz, A., Persson, P. B.,
875 et al. (2006). Translational control of collagen prolyl 4-hydroxylase-α(I)
876 gene expression under hypoxia. *J. Biol. Chem.* 281, 26089-26101. doi:
877 10.1074/jbc.M604939200

878 Feng, Z., Shen, Y., Wang, L., Cheng, L., Wang, J., Li, Q., et al. (2011). An
879 oligodeoxynucleotide with promising modulation activity for the
880 proliferation and activation of osteoblast. *Int. J. Mol. Sci.* 12, 2543-2555.
881 doi: 10.3390/ijms12042543
882 Fukada, S. I. (2018). The roles of muscle stem cells in muscle injury, atrophy
883 and hypertrophy. *J. Biochem.* 163, 353-358. doi: 10.1093/jb/mvy019
884 Girvan, A. C., Teng, Y., Casson, L. K., Thomas, S. D., Juliger, S., Ball, M. W.,
885 et al. (2006). AGRO100 inhibits activation of nuclear factor-kappaB (NF-
886 kappaB) by forming a complex with NF-kappaB essential modulator
887 (NEMO) and nucleolin. *Mol. Cancer Ther* 5, 1790-1799. doi: 10.1158/1535-
888 7163.MCT-05-0361
889 Gu, W., Schneider, J. W., Condorelli, G., Kaushal, S., Mahdavi, V., and Nadal-
890 Ginard, B. (1993). Interaction of myogenic factors and the retinoblastoma
891 protein mediates muscle cell commitment and differentiation. *Cell* 72, 309-
892 324. doi: 10.1016/0092-8674(93)90110-C
893 Guo, Y., Chen, Y., Wei, Y., Li, H., and Dong, C. (2015). Label-free fluorescent
894 aptasensor for potassium ion using structure-switching aptamers and
895 berberine. *Spectrochim. Acta A Mol. Biomol. Spectrosc.* 136 Pt C, 1635-
896 1641. doi: 10.1016/j.saa.2014.10.058
897 Harford, T. J., Kliment, G., Shukla, G. C., and Weyman, C. M. (2017). The
898 muscle regulatory transcription factor MyoD participates with p53 to
899 directly increase the expression of the pro-apoptotic Bcl2 family member
900 PUMA. *Apoptosis* 22, 1532-1542. doi: 10.1007/s10495-017-1423-x

Harford, T. J., Shaltouki, A., and Weyman, C. M. (2010). Increased expression of the pro-apoptotic Bcl2 family member PUMA and apoptosis by the muscle regulatory transcription factor MyoD in response to a variety of stimuli. *Apoptosis* 15, 71-82. doi: 10.1007/s10495-009-0428-5

Hartmann, G., Weeratna, R. D., Ballas, Z. K., Payette, P., Blackwell, S., Suparto, I., et al. (2000). Delineation of a CpG phosphorothioate oligodeoxynucleotide for activating primate immune responses in vitro and in vivo. *J. Immunol.* 164, 1617-1624. doi: 10.4049/jimmunol.164.3.1617

Hou, X., Shen, Y., Zhang, C., Zhang, L., Qin, Y., Yu, Y., et al. (2012). A specific oligodeoxynucleotide promotes the differentiation of osteoblasts via ERK and p38 MAPK pathways. *Int. J. Mol. Sci.* 13, 7902-7914. doi: 10.3390/ijms13077902

Huang, D. W., Sherman, B. T., and Lempicki, R. A. (2009). Systematic and integrative analysis of large gene lists using DAVID bioinformatics resources. *Nat. Protoc.* 4, 44-57. doi: 10.1038/nprot.2008.211

Iezzi, S., Di Padova, M., Serra, C., Caretti, G., Simone, C., Maklan, E., et al. (2004). Deacetylase inhibitors increase muscle cell size by promoting myoblast recruitment and fusion through induction of follistatin. *Dev. Cell* 6, 673-684. doi: 10.1016/S1534-5807(04)00107-8

Ikebe, J., Umezawa, K., Kamiya, N., Sugihara, T., Yonezawa, Y., Takano, Y., et al. (2011). Theory for trivial trajectory parallelization of multicanonical molecular dynamics and application to a polypeptide in water. *J. Comput. Chem.* 32, 1286-1297. doi: 10.1002/jcc.21710

924 Imenshahidi, M., and Hosseinzadeh, H. (2019). Berberine and barberry
925 (*Berberis vulgaris*): A clinical review. *Phytother. Res.* 33, 504-523. doi:
926 10.1002/ptr.6252
927 Jia, W., Yao, Z., Zhao, J., Guan, Q., and Gao, L. (2017). New perspectives of
928 physiological and pathological functions of nucleolin (NCL). *Life Sci.* 186,
929 1-10. doi: 10.1016/j.lfs.2017.07.025
930 Juliano, R. L. (2018). Intracellular trafficking and endosomal release of
931 oligonucleotides: What we know and what we don't. *Nucleic Acid Ther.* 28,
932 166-177. doi: 10.1089/nat.2018.0727
933 Kim, M., Sung, B., Kang, Y. J., Kim, D. H., Lee, Y., Hwang, S. Y., et al. (2015).
934 The combination of ursolic acid and leucine potentiates the differentiation
935 of C2C12 murine myoblasts through the mTOR signaling pathway. *Int. J.*
936 *Mol. Med.* 35, 755-762. doi: 10.3892/ijmm.2014.2046
937 Klinman, D., Shirota, H., Tross, D., Sato, T., and Klaschik, S. (2008).
938 Synthetic oligodeoxynucleotides as modulators of inflammation. *J. Leukoc.*
939 *Biol.* 84, 958-964. doi: 10.1189/jlb.1107775
940 Krieg, A. M., Yi, A. K., Matson, S., Waldschmidt, T. J., Bishop, G. A., Teasdale,
941 R., et al. (1995). CpG motifs in bacterial DNA trigger direct B-cell
942 activation. *Nature* 374, 546-549. doi: 10.1038/374546a0
943 Li, N., Liu, C., Mi, S., Wang, N., Zheng, X., Li, Y., et al. (2012). Simultaneous
944 determination of oleanolic acid, p-coumaric acid, ferulic acid, kaemperol
945 and quercetin in rat plasma by LC-MS-MS and application to a
946 pharmacokinetic study of *Oldenlandia diffusa* extract in rats. *J.*
947 *Chromatogr. Sci.* 50, 885-892. doi: 10.1093/chromsci/bms086

948 Litchfield, L. M., Riggs, K. A., Hockenberry, A. M., Oliver, L. D., Barnhart, K.
949 G., Cai, J., et al. (2012). Identification and characterization of nucleolin as
950 a COUP-TFII coactivator of retinoic acid receptor beta transcription in
951 breast cancer cells. *PLoS One* 7, e38278. doi: 10.1371/journal.pone.0038278
952 Losfeld, M. E., Khoury, D. E., Mariot, P., Carpentier, M., Krust, B., Briand, J.
953 P., et al. (2009). The cell surface expressed nucleolin is a glycoprotein that
954 triggers calcium entry into mammalian cells. *Exp. Cell Res.* 315, 357-369.
955 doi: 10.1016/j.yexcr.2008.10.039
956 Macke, T. J, and Case, D. A. (1998). "Modeling unusual nucleic acid
957 structures", in Molecular Modeling of Nucleic Acids, ed. Leontis, N. B., and
958 SantaLucia, J. (Washington DC: American Chemical Society), 379-393. doi:
959 10.1021/bk-1998-0682.ch024
960 Maier, J. A., Martinez, C., Kasavajhala, K., Wickstrom, L., Hauser, K. E., and
961 Simmerling, C. (2015). ff14SB: Improving the accuracy of protein side
962 chain and backbone parameters from ff99SB. *J. Chem. Theory Comput.* 11,
963 3696-3713. doi: 10.1021/acs.jctc.5b00255
964 Marchildon, F., Lamarche, E., Lala-Tabbert, N., St-Louis, C., and Wiper-
965 Bergeron, N. (2015). Expression of CCAAT/enhancer binding protein beta
966 in muscle satellite cells inhibits myogenesis in cancer cachexia. *PLoS One*
967 10, e0145583. doi: 10.1371/journal.pone.0145583
968 McCormick, R., and Vasilaki, A. (2018). Age-related changes in skeletal
969 muscle: changes to life-style as a therapy. *Biogerontology* 19, 519-536. doi:
970 10.1007/s10522-018-9775-3

971 Nigar, S., Yamamoto, Y., Okajima, T., Shigemori, S., Sato, T., Ogita, T., et al.
972 (2017). Synergistic oligodeoxynucleotide strongly promotes CpG-induced
973 interleukin-6 production. *BMC Immunol.* 18, 44. doi: 10.1186/s12865-017-
974 0227-7
975 Nihashi, Y., Ono, T., Kagami, H., and Takaya, T. (2019a). Toll-like receptor
976 ligand-dependent inflammatory responses in chick skeletal muscle
977 myoblasts. *Dev. Comp. Immunol.* 91, 115-122. doi:
978 10.1016/j.dci.2018.10.013
979 Nihashi, Y., Umezawa, K., Shinji, S., Hamaguchi, Y., Kobayashi, H., Kono, T.,
980 et al. (2019b). Distinct cell proliferation, myogenic differentiation, and gene
981 expression in skeletal muscle myoblasts of layer and broiler chickens. *Sci.*
982 *Rep.* 9, 16527. doi: 10.1038/s41598-019-52946-4
983 Norgaard, N. N., Holien, T., Jonsson, S., Hella, H., Espevik, T., Sundan, A., et
984 al. (2010). CpG-oligodeoxynucleotide inhibits Smad-dependent bone
985 morphogenetic protein signaling: effects on myeloma cell apoptosis and in
986 vitro osteoblastogenesis. *J. Immunol.* 185, 3131-3139. doi:
987 10.4049/jimmunol.0903605
988 Novitch, B. G., Mulligan, G. J., Jacks, T., and Lassar, A. B. (1996). Skeletal
989 muscle cells lacking the retinoblastoma protein display defects in muscle
990 gene expression and accumulate in S and G2 phases of the cell cycle. *J. Cell*
991 *Biol.* 135, 441-456. doi: 10.1083/jcb.135.2.441
992 Ou, T. M., Lu, Y. J., Tan, J. H., Huang, Z. S., Wong, K. Y., and Gu, L. Q. (2008).
993 G-quadruplexex: Targets in anticancer drug design. *ChemMedChem* 3,
994 690-713. doi: 10.1002/cmdc.200700300

995 Pohar, J., Lainscek, D., Fukui, R., Yamamoto, C., Miyake, K., Jerala, R., et al.
996 (2015). Species-specific minimal sequence motif for
997 oligodeoxyribonucleotides activating mouse TLR9. *J. Immunol.* 195, 4396-
998 4405. doi: 10.4049/jimmunol.1500600
999 Porrello, A., Cerone, M. A., Coen, S., Gurtner, A., Fontemaggi, G., Cimino, L.,
1000 et al. (2000). p53 regulates myogenesis by triggering the differentiation
1001 activity of pRb. *J. Cell Biol.* 151, 1295-1304. doi: 10.1083/jcb.151.6.1295
1002 Quemener, A. M., Bachelot, L., Forestier, A., Donnou-Fournet, E., Gilot, D.,
1003 and Galibert, M. D. (2020). The powerful world of antisense
1004 oligonucleotides: from bench to bedside. *Wiley Interdiscip. Rev. RNA* e1594.
1005 doi: 10.1002/wrna.1594
1006 Ramos, K. S., Moore, S., Runge, I., Tavera-Garcia, M. A., Cascone, I., Courty,
1007 J., et al. (2020). The nucleolin antagonist N6L inhibits LINE1
1008 retrotransposon activity in non-small cell lung carcinoma cells. *J. Cancer*
1009 11, 733-740. doi: 10.7150/jca.37776
1010 Reyes-Reyes, E. M., Salipur, F. R., Shams, M., Forsthoefel, M. K, and Bates,
1011 P. J. (2015). Mechanistic studies of anticancer aptamer AS1411 reveal a
1012 novel role for nucleolin in regulating Rac1 activation. *Mol. Oncol.* 9, 1392-
1013 1405. doi: 10.1016/j.molonc.2015.03.012
1014 Rubin, H. (2003). Cancer cachexia: its correlations and causes. *Proc. Natl.*
1015 *Acad. Sci. USA* 100, 5384-5389. doi: 10.1073/pnas.0931260100
1016 Ruijtenberg, S., and den Heuvel, S. (2016). Coordinating cell proliferation and
1017 differentiation: Antagonism between cell cycle regulators and cell type-
1018 specific gene expression. *Cell Cycle* 15, 196-212. doi:

10.1080/15384101.2015.1120925

Sackesen, C., van de Veen, W., Akdis, M., Soyer, O., Zumkehr, J., Ruckert, B., et al. (2013). Suppression of B-cell activation and IgE, IgA, IgG1 and IgG4 production by mammalian telomeric oligonucleotides. *Allergy* 68, 593-603. doi: 10.1111/all.12133

Shaltouki, A., Freer, M., Mei, Y., and Weyman, C. M. (2007). Increased expression of the pro-apoptotic Bcl2 family member PUMA is required for mitochondrial release of cytochrome C and the apoptosis associated with skeletal myoblast differentiation. *Apoptosis* 12, 2143-2154. doi: 10.1007/s10495-007-0135-z

Shen, Y., Feng, Z., Lin, C., Hou, X., Wang, X., Wang, J., et al. (2012). An oligodeoxynucleotide that induces differentiation of bone marrow mesenchymal stem cells to osteoblasts in vitro and reduces alveolar bone loss in rats with periodontitis. *Int. J. Mol. Sci.* 13, 2877-2892. doi: 10.3390/ijms13032877

Shinji, S., Nakamura, S., Nihashi, Y., Umezawa, K., and Takaya, T. (2020). Berberine and palmatine inhibit growth of human rhabdomyosarcoma cells. *Biosci. Biotechnol. Biochem.* 84, 63-75. doi: 10.1080/09168451.2019.1659714

Siddiqui-Jain, A., Grand, C. L., Bearss, D. J, and Hurley, L. H. (2002). Direct evidence for a G-quadruplex in a promoter region and its targeting with a small molecule to repress *c-MYC* transcription. *Proc. Natl. Acad. Sci. USA* 99, 11593-11598. doi: 10.1073/pnas.182256799

1042 Soddu, S., Blandino, G., Scardigli, R., Coen, S., Marchetti, A., Rizzo, M. G., et
1043 al. (1996). Interference with p53 protein inhibits hematopoietic and muscle
1044 differentiation. *J. Cell Biol.* 134, 193-204. doi: 10.1083/jcb.134.1.193
1045 Szklarczyk, D., Gable, A. L., Lyon, D., Junge, A., Wyder, S., Huerta-Cepas, J.,
1046 et al. (2019). STRING v11: protein-protein association networks with
1047 increased coverage, supporting functional discovery in genome-wide
1048 experimental datasets. *Nucleic Acids Res.* 47, D607-D613. doi:
1049 10.1093/nar/gky1131
1050 Takagi, M., Absalon, M. J., McLure, K. G., and Kastan, M. B. (2005).
1051 Regulation of p53 translation and induction after DNA damage by
1052 ribosomal protein L26 and nucleolin. *Cell* 123, 49-63. doi:
1053 10.1016/j.cell.2005.07.034
1054 Takaya, T., Nihashi, Y., Kojima, S., Ono, T., and Kagami, H. (2017).
1055 Autonomous xenogenic cell fusion of murine and chick skeletal muscle
1056 myoblasts. *Anim. Sci. J.* 88, 1880-1885. doi: 10.1111/asj.12884
1057 Tang, Z., Qiu, H., Luo, L., Liu, N., Zhong, J., Kang, K., et al. (2017). miR-34b
1058 modulates skeletal muscle cell proliferation and differentiation. *J. Cell.*
1059 *Biochem.* 118, 4285-4295. doi: 10.1002/jcb.26079
1060 Teng, Y., Girvan, A. C., Casson, L. K., Pierce, W. M. Jr, Qian, M., Thomas, S.
1061 D., et al. (2007). AS1411 alters the localization of a complex containing
1062 protein arginine methyltransferase 5 and nucleolin. *Cancer Res.* 67, 10491-
1063 10500. doi: 10.1158/0008-5472.CAN-06-4206

1064 Tsui, V., and Case, D. A. (2000). Theory and applications of the generalized
1065 born solvation model in macromolecular simulations. *Biopolymers* 56, 275-
1066 291. doi: 10.1002/1097-0282(2000)56:4<275::AID-BIP10024>3.0.CO;2-E
1067 Vollmer, J., and Krieg, A. M. (2009). Immunotherapeutic applications of CpG
1068 oligodeoxynucleotide TLR9 agonists. *Adv. Drug Deliv. Rev.* 61, 195-204. doi:
1069 10.1016/j.addr.2008.12.008
1070 Wang, H., Chen, Y., Lu, X. A., Liu, G., Fu, Y., and Luo, Y. (2015). Endostatin
1071 prevents dietary-induced obesity by inhibiting adipogenesis and
1072 angiogenesis. *Diabetes* 64: 2442-2456. doi: 10.2337/db14-0528/-/DC1
1073 Wang, J., Wolf, R. M., Caldwell, J. W., Kollman, P. A., Case, D. A. (2004).
1074 Development and testing of a general amber force field. *J. Comput. Chem.*
1075 25, 1157-1174. doi: 10.1002/jcc.20035
1076 Wang, T., Chen, C., Larcher, L. M., Barrero, R., and Veedu, R. N. (2019). Three
1077 decades of nucleic acid aptamer technologies: Lessons learned, progress
1078 and opportunities on aptamer development. *Biotechnol. Adv.* 37, 28-50. doi:
1079 10.1016/j.biotechadv.2018.11.001
1080 Wang, Y., Yamamoto, Y., Shigemori, S., Watanabe, T., Oshiro, K., Wang, X., et
1081 al. (2015). Inhibitory/suppressive oligodeoxynucleotide nanocapsules as
1082 simple oral delivery devices for preventing atopic dermatitis in mice. *Mol.*
1083 *Ther.* 23, 297-309. doi: 10.1038/mt.2014.239
1084 Yamamoto, Y., Sugimura, R., Watanabe, T., Shigemori, S., Okajima, T., Nigar,
1085 S., et al. (2017). Class A CpG oligodeoxynucleotide priming rescues mice
1086 from septic shock via activation of platelet-activating factor
1087 acetylhydrolase. *Front. Immunol.* 8, 1049. doi: 10.3389/fimmu.2017.01049

1088 Yang, G., Wan, M., Zhang, Y., Sun, L., Sun, R., Hu, D., et al. (2010). Inhibition
1089 of a C-rich oligodeoxynucleotide on activation of immune cells in vitro and
1090 enhancement of antibody response in mice. *Immunology* 131, 501-512. doi:
1091 10.1111/j.1365-2567.2010.03322.x
1092 Yazidan-Robati, R., Bayat, P., Oroojalian, F., Zargari, M., Ramezani, M.,
1093 Taghdisi, S. M., et al. (2019). Therapeutic applications of AS1411 aptamer,
1094 an update review. *Int. J. Biol. Macromol.* 155, 1420-1431. doi:
1095 10.1016/j.ijbiomac.2019.11.118
1096 Yu, G., and He, Q. Y. (2016). ReactomePA: an R/Bioconductor package for
1097 reactome pathway analysis and visualization. *Mol. BioSyst.* 12, 477-479.
1098 doi: 10.1039/C5MB00663E
1099 Zhang, L., Wang, X. H., Wang, H., Du, J., and Mitch, W. E. (2010). Satellite
1100 cell dysfunction and impeired IGF-1 signaling cause CKD-induced muscle
1101 atrophy. *J. Am. Soc. Nephrol.* 21, 419-427. doi: 10.1681/ASN.2009060571
1102 Zou, W., Amcheslavsky, A., amd Bar-Shavit, Z. (2003). CpG
1103 oligodeoxynucleotides modulate the osteoclastogenic activity of osteoblasts
1104 via Toll-like receptor 9. *J. Biol. Chem.* 278, 16732-16740. doi:
1105 10.1074/jbc.M212473200
1106

Figure Legends

Figure 1. Identification of myoDNs. (**A**) Ratio of MHC$^+$ cells within the screened mMBs treated with 10 μM PS-ODNs in GM for 48 h (screening system). ** $p < 0.01$ (Dunnett's test). $n = 3$. (**B**) Representative immunofluorescent images of the hMBs treated with 10 μM iSN04 in DM for 48 h. Scale bar, 200 μm. Ratio of MHC$^+$ cells and multinuclear myotubes were quantified. ** $p < 0.01$ (Student's t test). $n = 6$. (**C**) Relative numbers of the mMBs and MEFs treated with 1 or 3 μM iSN04 in GM for each cell. Mean value of the control sample at 0 h was set to 1.0 for each experiment. * $p < 0.05$, ** $p < 0.01$ vs control at each time point (William's test). $n = 3$. (**D**) qPCR results of myogenic gene expression in the hMBs treated with 30 μM iSN04 in DM for 24 h. Mean value of control hMBs was set to 1.0. * $p < 0.05$, ** $p < 0.01$ vs control (Student's t test). $n = 3$. (**E**) Representative fluorescent images of the hMBs treated with 5 μg/ml 6-FAM-iSN04 in GM. Scale bar, 100 μm. (**F**) MHC signal intensities of the hMBs treated with 30 μM of iSN04, CpG-2006, or Tel-ODN in DM for 48 h (screening system). NS, no significant difference (Scheffe's F test). $n = 3$.

Figure 2. Profile of iSN04-dependent gene expression. (**A**) Scattered plot of the 476 iSN04-upregulated DEGs significantly ($p < 5.0\times10^{-3}$) enriched in GO terms. (**B**) Scattered plot of the 423 iSN04-downregulated DEGs significantly ($p < 5.0\times10^{-6}$) enriched in GO terms. (**C**) Functional and physiological

networks within the 476 iSN04-upregulated DEGs (left panel) and the 423 iSN04-downregulated DEGs (right panel) visualized via STRING analysis.

Figure 3. Berberine enhances iSN04 activity by causing a shift in molecular structure. (**A**) The conformation of iSN04 simulated via TTP-McMD. (**B**) Contact map of iSN04. The scale indicates contact probability. (**C**) The simulated conformation of iSN04-berberine complex. Berberine is shown as a sphere model. (**D**) Contact map of iSN04-berberine complex. "B" indicates berberine. (**E**) Representative images of agarose gel electrophoresis of iSN04 mixed with berberine (Ber) in F10 medium. The EtBr-stained and UV-irradiated gel was scanned without filters (upper image) and with a 560-nm filter (lower image). (**F**) Ratio of MHC^+ cells within the mMBs treated with 10 μM iSN04 and 10 μM berberine in GM for 48 h (screening system). ** $p < 0.01$; NS, no significant difference (Scheffe's F test). $n = 3$. (**G**) Ratio of MHC^+ cells within the mMBs treated with 10 μM of mutant iSN04 in GM for 48 h (screening system). * $p < 0.05$, ** $p < 0.01$ vs control; †† $p < 0.01$ vs iSN04 (Scheffe's F test). $n = 3$. (**H**) Ratio of MHC^+ cells within the mMBs treated with 0, 1, or 3 μM iSN04 and 0, 1, 3, 10, or 30 μM of berberine in GM for 48 h (screening system). * $p < 0.05$ vs 0 μM-iSN04 + 0 μM-berberine; † $p < 0.05$, †† $p < 0.01$ vs 3 μM-iSN04 + 0 μM-berberine (Scheffe's F test). $n = 3$. (**I**) Representative images of agarose gel electrophoresis of mutant iSN04 mixed with berberine in F10 medium. (**J**) Representative images of agarose gel electrophoresis of iSN04 mixed with coptisine (Cop), berberine, palmatine (Pal), or jatrorrhizine (Jat) in F10 medium. (**K**) Ratio of MHC^+ cells within

1154 the mMBs treated with 10 μM iSN04 and 10 μM berberine analogs in GM for
1155 48 h (screening system). * $p < 0.05$ vs control-iSN04(-); †† $p < 0.01$ vs control-
1156 iSN04(+) (Tukey-Kramer test). $n = 3$.
1157
1158 **Figure 4.** iSN04 targets nucleolin and improves p53 protein level. (**A**)
1159 Representative image of CBB-stained SDS-PAGE gel of the ODN-precipitated
1160 proteins. The arrow indicates the bands subjected to mass spectrometry. (**B**)
1161 Representative immunofluorescent images of the hMBs treated with 10 μM
1162 of iSN04 or AS1411 in DM for 48 h. Scale bar, 200 μm. Ratio of MHC^+ cells
1163 and multinuclear myotubes were quantified. ** $p < 0.01$ vs control; NS, no
1164 significant difference (Student's t test). $n = 6$. (**C**) Representative
1165 immunofluorescent images of the hMBs maintained in DM at day 0, 2, and 4.
1166 Scale bar, 50 μm. (**D**) Representative immunofluorescent images of the hMBs
1167 treated with 30 μM of iSN04 or AS1411 in DM for 48 h. Scale bar, 50 μm. (**E**)
1168 Scattered plot of the 899 iSN04-dependent DEGs significantly (FDR $p < 0.05$)
1169 enriched in KEGG pathways. (**F**) Representative images of Western blotting
1170 (10 μg protein/lane) of p53, nucleolin, and GAPDH in soluble whole cell
1171 lysates of the hMBs treated with 30 μM of iSN04 or AS1411 in DM for 48 h.
1172 Amounts of p53 and nucleolin were normalized using GAPDH. Mean value of
1173 control hMBs was set to 1.0. * $p < 0.05$, ** $p < 0.01$ vs control (Scheffe's F test).
1174 $n = 3$.

Figure 1

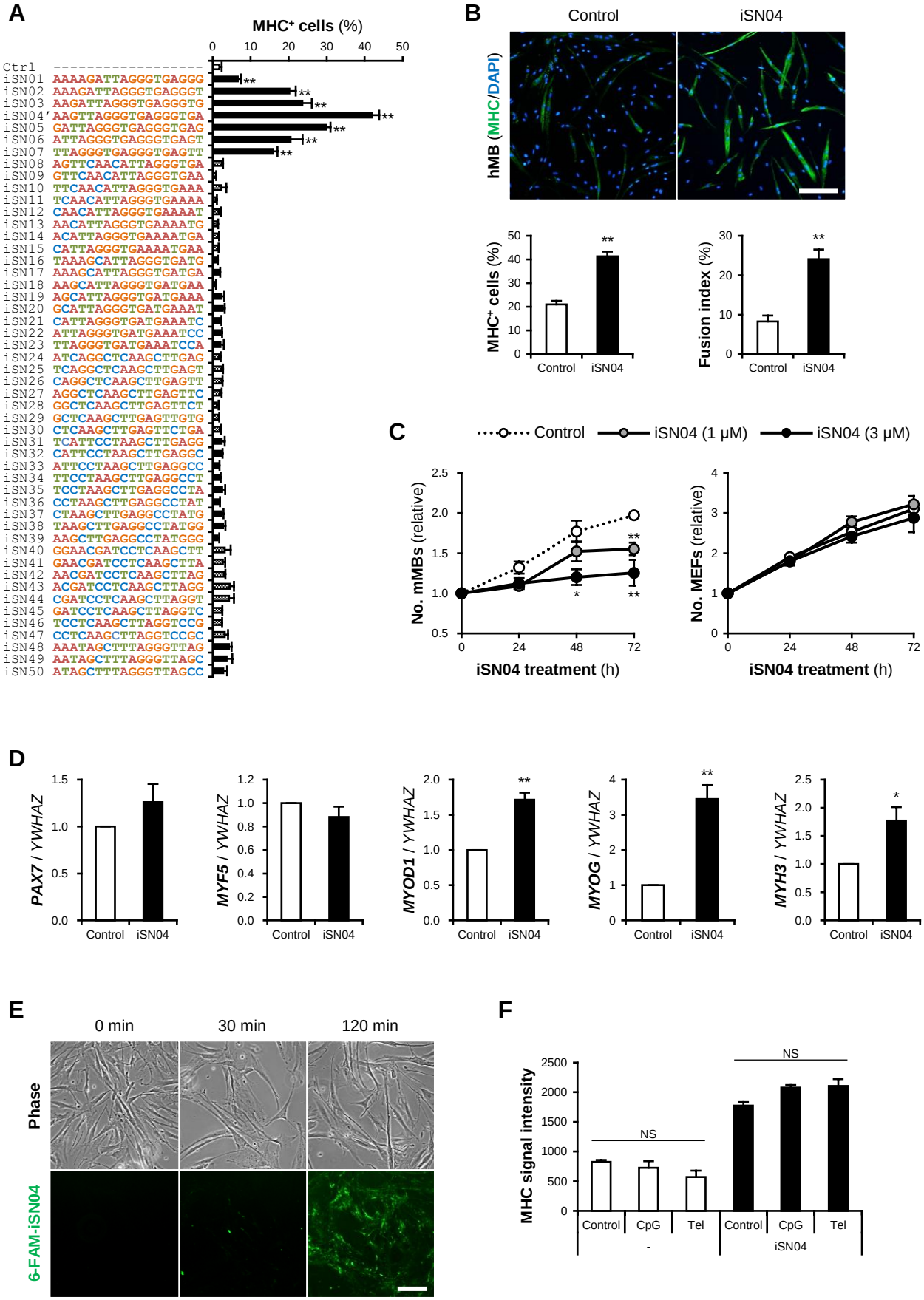

Figure 2

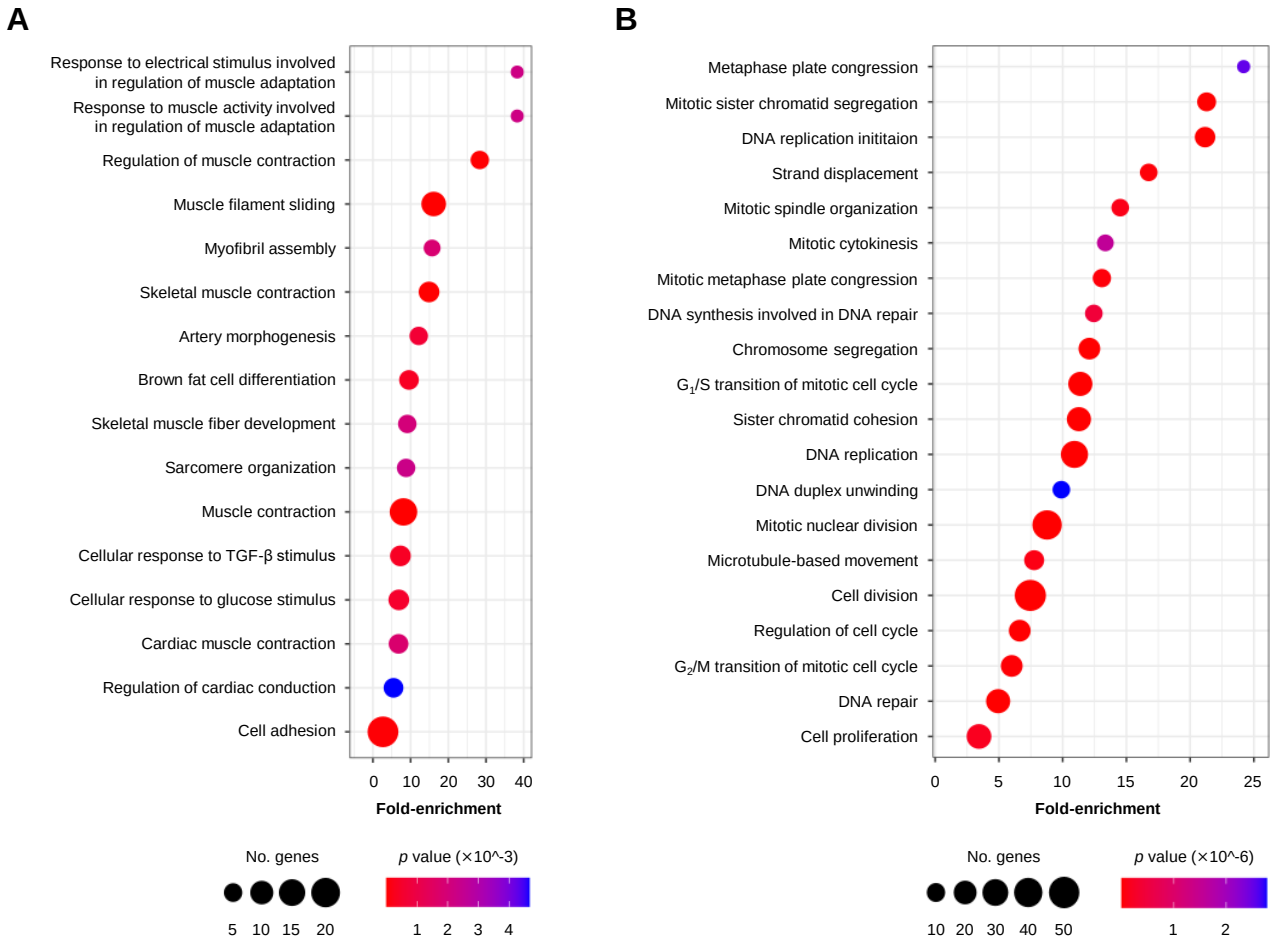

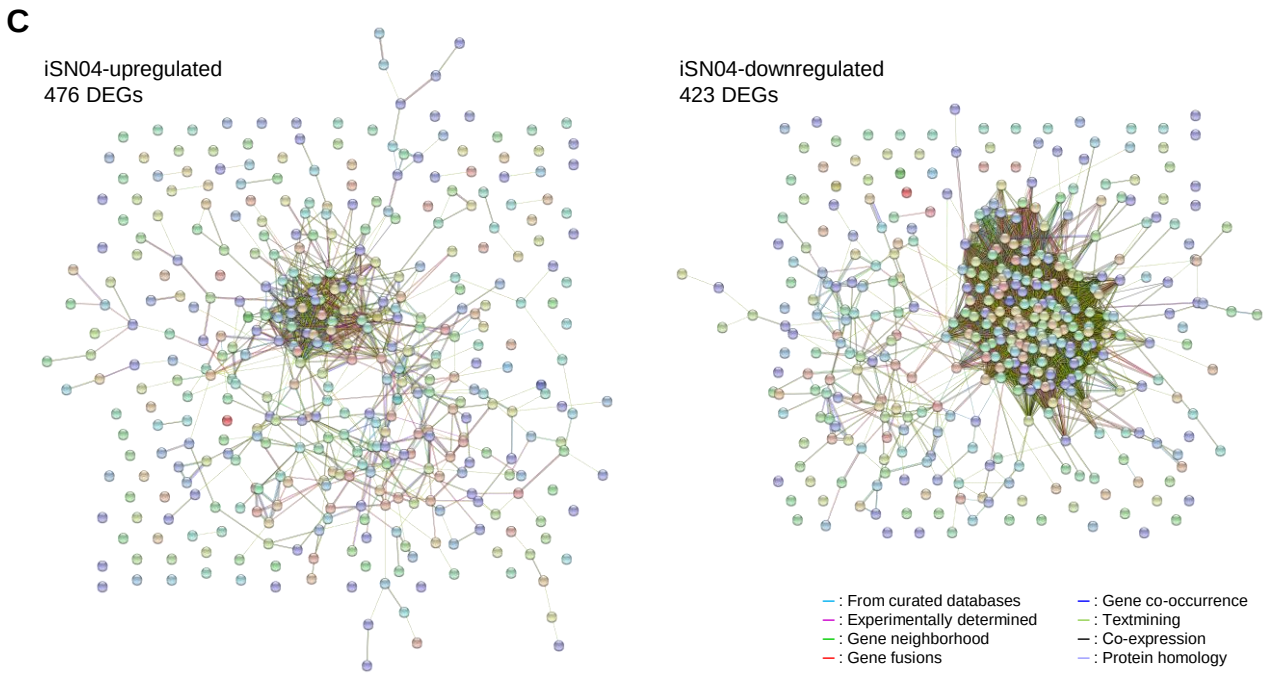

Figure 3

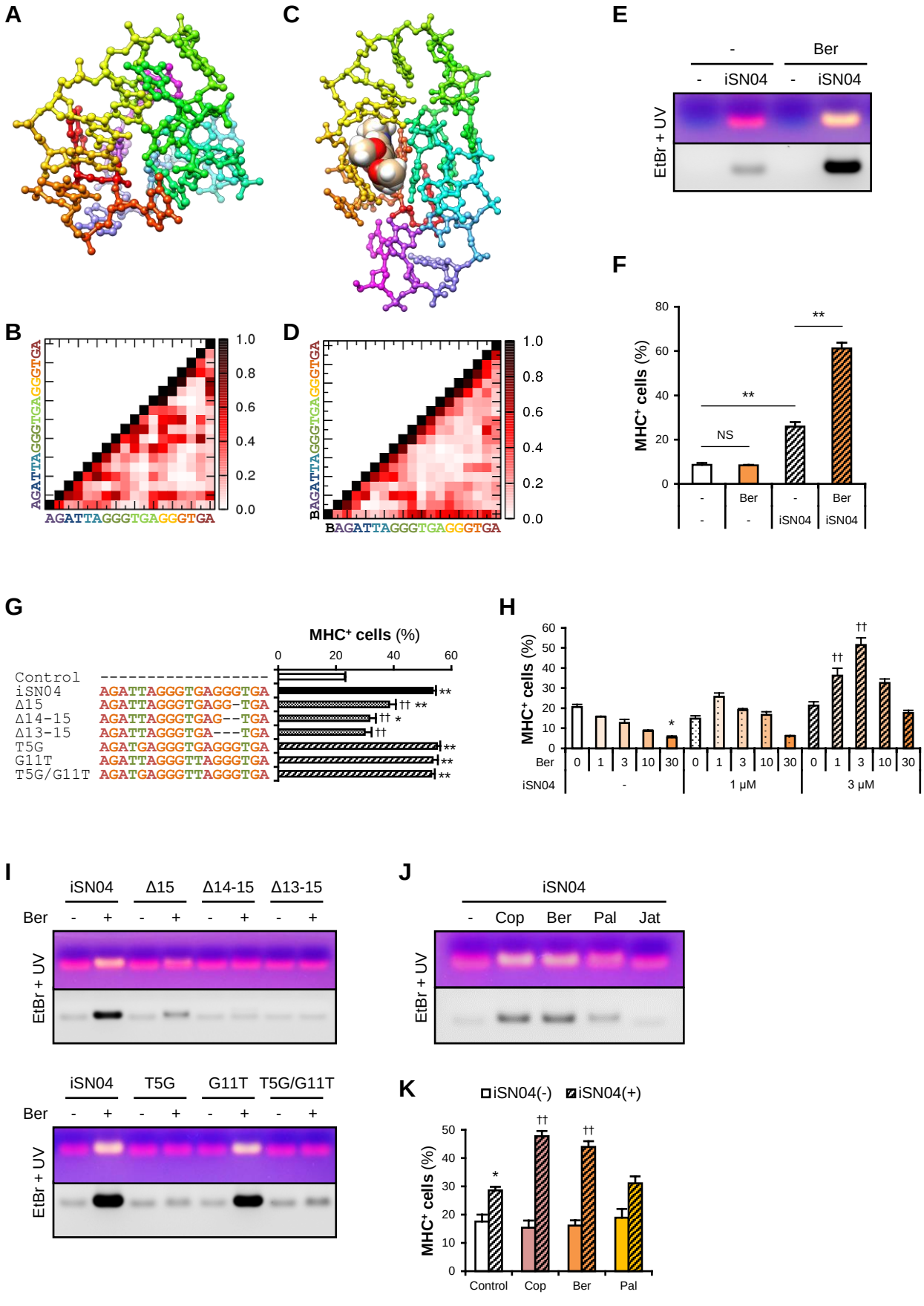

Figure 4